2019

Identification of Nucleate Boiling as the Dominant Heat Transfer Mechanism during Confined Two-Phase Jet Impingement

M. D. Clark
Purdue University

J. A. Weibel
Purdue University, jaweibel@purdue.edu

S V. Garimella
Purdue University, sureshg@purdue.edu

Clark, M. D.; Weibel, J. A.; and Garimella, S V., "Identification of Nucleate Boiling as the Dominant Heat Transfer Mechanism during Confined Two-Phase Jet Impingement" (2019). *CTRC Research Publications.* Paper 333.
http://dx.doi.org/https://doi.org/10.1016/j.ijheatmasstransfer.2018.09.058

Identification of nucleate boiling as the dominant heat transfer mechanism during confined two-phase jet impingement[1]

Matthew D. Clark, Justin A. Weibel, Suresh V. Garimella[2]
Cooling Technologies Research Center, School of Mechanical Engineering
Purdue University, 585 Purdue Mall, West Lafayette, IN 47907 USA

Abstract

Thermal management of high-power electronics requires cooling strategies capable of dissipating high heat fluxes while maintaining the device at low operating temperatures. Two-phase jet impingement offers a compact cooling technology capable of meeting these requirements at a low pressure drop. Generally, confined impingement geometries are used in electronics cooling applications, where the flow is constrained between the hot surface and orifice plate. Understanding the primary heat transfer mechanisms occurring as boiling takes place on the surface during jet impingement is important, specifically under such confined conditions. In this study, heat transfer from a copper surface is experimentally characterized in both confined jet impingement and pool boiling configurations. The dielectric liquid HFE-7100 is used as the working fluid. For the jet impingement configuration, the jet issues through a single 2 mm-diameter orifice, at jet exit velocities of 1, 3, 6, and 9 m/s, into a confinement gap with a spacing of 3 jet diameters between the orifice and heat source. Additional orifice-to-target spacings of 0.5, 1, and 10 jet diameters are tested at the lowest (V_j = 1 m/s) and highest (V_j = 9 m/s) jet velocities. By incrementing the heat flux applied to the surface and observing the steady-state response at each flux, the single-phase and two-phase heat transfer performance is characterized; all experiments were carried through to critical heat flux conditions. The jet impingement data in the fully boiling regime either directly overlap the pool boiling data, or coincide with an extension of the trend in pool boiling data beyond the pool boiling critical heat flux limit. This result confirms that nucleate boiling is the dominant heat transfer mechanism in the fully boiling regime in confined jet impingement; the convective effects of the jet play a negligible role over the wide range of parameters considered here. While the presence of the jet does not enhance the boiling heat transfer coefficient, the jet does greatly increase single-phase heat transfer performance and extends the critical heat flux limit. Critical heat flux displays a linear dependence on jet velocity while remaining insensitive to changes in the orifice-to-target spacing.

---

[1] Submitted for possible publication in *International Journal of Heat and Mass Transfer*, 2018.
[2] Corresponding author, Tel.: +1 765 494 5621. E-mail address: sureshg@purdue.edu.

Keywords

Electronics cooling, jet impingement, pool boiling, two-phase heat transfer, critical heat flux

Nomenclature

A	heat source area
Bl^*	non-dimensional heat input $qA/\dot{m}C_p(T_{sat}-T_j)$
CHF	critical heat flux
C_p	specific heat
d	orifice diameter
H	orifice-to-target spacing
$\bar{h}$	area-averaged heat transfer coefficient
h_{fh}	latent heat of vaporization
l	orifice plate thickness
$\dot{m}$	mass flow rate
p_{op}	operating pressure
q	heat flux
Ra	average surface roughness
Re	Reynolds number ($\rho v_j d / \mu$)
T	temperature
$\bar{T}$	area-averaged temperature
ΔT_{sub}	degree of subcooling (T_{sat} - T_j)
$\dot{V}$	volumetric flow rate
V_j	jet exit velocity

Greek symbols

μ	liquid dynamic viscosity
ρ	liquid density

Subscript

CHF	critical heat flux limit
j	jet exit condition
s	surface condition
sat	saturated condition

1 Introduction

Two-phase jet impingement heat transfer is a viable method for thermal management of high-density electronics systems. Due to the large number of adjustable geometric parameters and operating conditions, jet impingement systems can be designed for low-pressure-drop operation while maintaining high levels of heat dissipation [1]. Confined outlet conditions, where the jet issues into a gap bounded by the heated surface and an orifice plate, are typical in electronics cooling applications due to compact packaging constraints.

The heat transfer regimes observed in two-phase jet impingement as the surface heat flux increases include: a single-phase regime before incipience, a partial boiling regime, and a fully boiling regime, followed by critical heat flux (CHF). During the partial boiling regime, boiling initiates at the periphery of the heated surface and traverses inward towards the jet axis with increasing heat flux. Consequently, both single-phase and nucleate boiling heat transfer exist simultaneously on the heated surface during this regime [2–6]. Once the boiling front reaches the jet axis, boiling occurs over the entire surface in the fully boiling regime. The fully boiling regime is a desirable operating condition, because substantial increases in heat flux are accompanied by only modest surface temperature increases in this regime. A better understanding of the dominant heat transfer mechanisms that govern performance in the fully boiling regime can help direct predictive modeling efforts. It is also important to understand the dependence of the CHF limit on the geometric parameters and operating conditions of the impinging jet, such as orifice-to-target spacing and jet velocity.

Two heat transfer modes are present during two-phase jet impingement: forced convection and nucleate boiling. To better understand how the impinging jet affects performance, a direct comparison with pool boiling heat transfer, where forced convection effects are absent, is useful as a benchmark. Though significant experimental work has been performed on two-phase jet impingement heat transfer, few experimental studies have directly compared jet impingement heat transfer with pool boiling, and none have considered confined jets. Katto and Kunihiro [7], Bergles and Ma [8,9], Struble and Witte [10], and Zhou and Ma [11] reported experimental comparisons of pool boiling and submerged, unconfined jet impingement. In each of these studies, the jet impingement data in the fully boiling regime coincided with the pool boiling curve. An exception found by Bergles and Ma [9] was attributed to their extensive extrapolation of the pool boiling data to draw a comparison at heat fluxes above their measured pool boiling data.

In recent work by Mira-Hernández *et al.* [5], a semi-empirical model for predicting area-averaged two-phase heat transfer from confined impinging jets was developed. The model, which treats single-phase and boiling regions on the surface separately, used nucleate pool boiling correlations to predict the local heat transfer coefficient in regions of the surface undergoing boiling under the jet. The model accurately

predicted jet impingement experimental data in the fully boiling regime [5], without including any convection effects. This result calls for an experimental investigation that directly compares confined jet impingement boiling behavior with nucleate pool boiling heat transfer.

The present study performs experiments that characterize heat transfer from a surface under both confined jet impingement and pool boiling conditions. In the jet impingement configuration, a single 2 mm-diameter orifice is used; the jet velocity (V_j = 1 m/s, 3 m/s, 6 m/s, and 9 m/s) and orifice-to-target spacing (H/d = 0.5, 1, 3, and 10) are varied. Comparison of jet impingement heat transfer in the fully boiling regime to pool boiling provides insight into the effect of impingement on boiling heat transfer and reveals that even at high jet velocities, convective effects do not have an influence on the heat transfer coefficient. The effect of the impinging jet on critical heat flux is also discussed; trends in critical heat flux with respect to jet velocity are identified.

2 Experimental methods

Experiments are performed using a two-phase flow loop charged with the dielectric fluid HFE-7100 [12]. The test section is reconfigurable to allow characterization of both jet impingement and pool boiling heat transfer. Details of the experimental facility, procedures, and data reduction are described in this section.

2.1 Flow loop

The flow loop used to perform the experiments is described in detail in Ref. [13] and is shown schematically in Figure 1(c). A magnetically coupled gear pump circulates fluid through the flow loop. The flow rate is coarsely set by adjusting the rotational speed of the pump and finely tuned by metering the flow through a bypass loop and the test section. Mass flow rate is measured by a Coriolis flow meter (CMFS015, Emerson) with ±0.1% accuracy. Any plasticizers or organic contaminants are removed from the working fluid using an activated carbon filter while particulates are removed using 0.5 μm particulate filters. The liquid subcooling is controlled by adjusting the voltage supplied to the 1.2 kW inline preheater. Fluid exits the test section and is returned to the fluid reservoir; for degassing purposes, the reservoir is equipped with a 1 kW immersion heater and two Graham reflux condensers. A copper-finned liquid-to-air heat exchanger equipped with a voltage-regulated fan is used to cool the fluid before the pump inlet; this prevents cavitation in the pump and provides greater control over the test section inlet temperature.

2.2 Test section

The test section, modified from the original heater assembly used in Ref. [4], is shown schematically in Figure 1(a). The side walls are made of polyether ether ketone (PEEK) for thermal insulation, while the front and back walls are made of polycarbonate for optical access, allowing high-speed visualizations through the side of the test section. Fluid enters the top of the circular cross-section plenum and passes through two screens and a honeycomb to straighten the flow. The test section inlet pressure and temperature are measured by a pressure tap and a T-type thermocouple placed close to the orifice plate inside the plenum. The circular plenum is sealed to the top of the test section by an O-ring, allowing the plenum to translate vertically so that its position can be adjusted.

For the jet impingement configuration (see Figure 1(b)), an orifice plate with a single 2 mm-diameter orifice located at the center of the plate is mounted to the bottom of the plenum and sealed by an O-ring. A single jet is chosen instead of a jet array in order to maximize the possible range of jet velocities and orifice-to-target spacing ratios that can be tested given the ranges of the pump and sensors used in the experimental facility. The orifice aspect ratio (l/d) is chosen to be 2, to minimize pressure drop according to Ref. [14]. The orifice-to-target spacing (H) is precisely set by spacer pins inserted into the bottom of the test section and the exit face of the orifice plate.

To enable a pool boiling configuration (see Figure 1(b)), the subcooled inlet flow is diverted radially outward by a solid plate mounted 1.5 mm away from the end of the plenum. The exit area is over 100 times that of the 2 mm-diameter jet and results in an exit velocity of 0.01 m/s for the inlet flow rate used (188 ml/min), which prevents any forced flow near the heater surface. Additionally, the plenum is raised to its maximum height for this case. High-speed videos acquired during the pool boiling experiments, which are included in the Supplementary Materials, show no apparent convection in the test chamber near the heater surface.

Fluid exits the plenum into the submerged chamber bath and leaves the test section through an exit port in the top wall (Figure 1(a)). The chamber pressure is measured with a pressure tap (Gems 2200BG3F002A3UA) located in the bottom of the test section. A T-type thermocouple inserted into the side wall of the test section allows measurement of the fluid bath temperature.

The square heat transfer surface is the top of a 20 mm × 20 mm × 37 mm oxygen-free copper block heated by twelve 100 W cartridge heaters inserted into the bottom. The copper block is equipped with three thermocouple rakes located along the centerline and near two opposing sidewalls, allowing for estimation of the average surface temperature by extrapolation. The centerline thermocouple rake includes four T-type thermocouples spaced at 2.54 mm increments. The near-sidewall thermocouple rakes include two T-type thermocouples each, vertically separated by 7.62 mm. To reduce heat loss, fiberglass insulation is loosely packed in the cavity between the copper block and the surrounding PEEK carrier.

The copper block is supported from below by a ceramic block, which prevents high-temperature exposure of the PEEK and provides additional insulation. After ensuring that the top surface of the copper block is flush with the surrounding 4 mm-thick PEEK plate, the top edge of the heater is sealed in place (Q3-6611, Dow Corning).

2.3 Experimental procedure

Prior to the start of an experiment, the HFE-7100 is thoroughly degassed by cycling fluid at a flow rate of 300 ml/min through the loop while boiling the fluid using the inline heater and reservoir immersion heaters. Noncondensable gases are allowed to escape through the reflux condensers, while vapor is condensed and returns to the reservoir. This degassing procedure is carried out for 2 h before each experiment. During each test, the facility is run in an open-loop configuration while using the immersion heater to maintain saturation temperature in the reservoir at atmospheric pressure (101.3 kPa); the noncondensable gases continue to be vented. This ensures that the fluid remains degassed throughout the length of the experiment.

After adjusting the flow rate to the desired value, the inlet subcooling is set at 8 °C relative to the saturation temperature calculated using the measured test section chamber pressure. Power to the copper heater block is incremented in steps of 8 W for jet exit velocities of 1 m/s and 3 m/s and steps of 24 W for jet exit velocities of 6 m/s and 9 m/s, and steady-state data are recorded when a change of less than 1 °C/h in the average surface temperature is measured. Data are acquired at a frequency of 0.5 Hz for 2 min, providing approximately 60 data points that are averaged and reported as steady-state values for each recorded power step. During steady-state operation, high-speed videos are acquired from the side of the test section (Phantom VEO 710L) at 3000 fps. Table 1 summarizes all of the jet impingement experimental operating conditions.

When using a highly wetting fluid such as HFE-7100, temperature overshoot at boiling incipience is often observed [13], as in the low jet velocity cases of the current study (V_j = 1 and 3 m/s). This is caused by the wetting fluid filling the cavities in a surface, resulting in an increased superheat temperature requirement for nucleation to occur compared to a less wetting fluid [15]. The exact superheat temperature at which incipience occurs can vary according to a number of factors, such as the rest time between boiling experiments [16], and is generally characterized by a probabilistic representation [17]. Using the smooth surface with a roughness (Ra) of 0.5 μm, in one of the current experiments (V_j = 3 m/s; H/d = 3), an extreme temperature overshoot led to film boiling upon incipience; in this case, the heater power is reduced until the surface returns to nucleate boiling conditions and the test is resumed as normal.

All tests were carried through to a critical heat flux condition, marked by a rapid surface temperature excursion upon incrementing power to the heater. The critical heat flux values are extracted from the

transient data immediately prior to the rapid temperature excursion. The last data point presented in each curve corresponds to this critical heat flux value.

2.4 Data reduction and uncertainty

The surface temperature of the copper heater is extrapolated from the temperature gradient measured using the three thermocouple rakes inside the block. Thermocouple measurement uncertainties are estimated to be ±0.3 °C, while the surface temperature extrapolation resulted in an uncertainty of ±0.44 °C at low heat fluxes to ±0.87 °C at the highest recorded heat flux of 82.4 W/cm^2. A numerical model [13] is used to estimate the heat loss from the block. This heat loss is subtracted from the measured electrical power supplied to the heater for calculation of heat flux into the fluid. Uncertainty in heat flux was estimated to be less than 2% based on a 95% confidence interval. All uncertainties are calculated as described in Ref. [13].

3 Results

Boiling curves showing the average superheat ($\bar{T}_s - T_{sat}$) as a function of heat flux are shown in the left panels of Figure 2 and Figure 3, while area-averaged heat transfer coefficients are shown in the right panels, also as a function of heat flux. Results obtained in the jet impingement experimental configuration are compared to the baseline pool boiling data. The boiling curves in the jet impingement configuration, follow the same general trends for all cases, which are first introduced here. A shallow slope in the heat flux versus average superheat at the lowest heat fluxes, corresponding to single-phase jet impingement, is followed by a steeper slope at higher heat fluxes during two-phase jet impingement after boiling incipience. Ultimately, CHF occurs and is denoted by a horizontal arrow that terminates the boiling curve. The heat transfer coefficients are constant during the single-phase regime at lower heat fluxes, followed by a near-linear increase with heat flux throughout the two-phase regime. For the boiling curve obtained in the pool boiling experimental configuration, data at low heat fluxes corresponding to the natural convection regime are omitted for clarity; all pool boiling data shown are in the nucleate boiling regime.

3.1 Effect of jet velocity

Figure 2(a) shows boiling curves corresponding to four different jet velocities ranging from 1 m/s to 9 m/s at a single, fixed orifice-to-target spacing (*H/d* = 3). As the jet velocity is increased, the single-phase wall superheat is significantly lower at a given heat flux (*i.e.*, the boiling curve has a steeper slope), as would be expected of single-phase jet impingement [18]. Once boiling occurs during jet impingement, the data corresponding to all four jet velocities collapse to a single characteristic curve; the surface superheat during the fully boiling regime is insensitive to the jet velocity over this range. Furthermore,

this characteristic behavior matches the trend of the pool boiling data. These boiling curve trends are reflected in the heat transfer coefficients as well. The single-phase average heat transfer coefficient increases with jet velocity, and in the fully boiling regime, the curves corresponding to all four jet velocities converge. To illustrate that the characteristic heat transfer coefficient behavior during two-phase jet impingement follows that of pool boiling, a curve of the form $\bar{h} = cq^n$ is fit to the pool boiling data. This functional form is common to pool boiling correlations in the literature [19,20]. This curve is plotted as the red dashed line in Figure 2(b), extended to heat fluxes beyond the pool boiling CHF for reference. Even at the highest jet velocity of 9 m/s, the heat transfer coefficient closely matches the trend fitted to the pool boiling data. This unequivocally demonstrates that the fully boiling regime heat transfer coefficient is predominantly governed by a nucleate boiling heat transfer mechanism and is unaffected by the impinging jet, reaffirming that fully boiling regime performance can be predicted via nucleate boiling correlations [5].

The impinging jet does, however, result in an extension of the critical heat flux because of the added momentum provided by the jet velocity. Figure 4 plots CHF as a function of jet velocity for a confinement height of 3 jet diameters. The pool boiling critical heat flux is also shown for reference. A cube-root relationship of CHF with jet velocity ($q_{CHF} \sim V_j^{1/3}$) has been commonly reported for free-surface and submerged jets [21,22]. In comparison, there has been very little investigation of the CHF trends for highly confined jet impingement, with the only report being a stronger dependence of CHF on jet velocity ($q_{CHF} \sim V_j^{0.6}$) for a confined ($0.508 \leq H \leq 5.08\ mm$), planar jet of FC-72 [23]. The current study, as shown in Figure 4, points to a near-linear dependence of CHF on jet velocity.

3.2 Effect of orifice-to-target spacing

Boiling curves and heat transfer coefficients corresponding to jet velocities of 1 m/s and 9 m/s for orifice-to-target spacings of 0.5, 1, 3, and 10 jet diameters are shown in Figure 3.

For the higher jet velocity (V_j = 9 m/s), in the single-phase regime of the boiling curves (Figure 3(a)), there is little difference in performance between the orifice-to-target spacings of 0.5, 1, and 3 jet diameters. There is a degradation in single-phase performance for the highest orifice-to-target spacing (*H/d* = 10), which has been observed in the literature for spacings beyond 5–8 diameters [24]. Once boiling occurs, the curves corresponding to orifice-to-target spacings of 1, 3, and 10 diameters converge to match the behavior of the pool boiling data, as was observed in Figure 2(a). However, the smallest orifice-to-target spacing (*H/d* = 0.5) resulted in a significant degradation of performance in the fully boiling regime. Above 46.3 W/cm^2, the boiling curve slope changes at this spacing and the wall superheat exceeds that of all the higher orifice-to-target spacings, until ultimately terminating in a significantly

lower CHF (57.6 W/cm^2) than the other cases. Unlike all other boiling curves, the heat transfer coefficient decreases with increasing heat flux within this range. To the authors' knowledge, this dramatic reduction in performance has not yet been observed in the literature and could be due to vapor confinement at the very low spacing of 0.5 jet diameters (H = 1 mm for d = 2 mm). The small confinement gap does not allow for clear conclusions to be drawn from visualization of the two-phase flow.

Due to the significantly lower jet velocity, the jet impingement boiling curves corresponding to V_j = 1 m/s (Figure 3(c)) barely change from the pool boiling data in terms of the CHF limit and show little difference between the four orifice-to-target spacings. A maximum CHF of 27.8 W/cm^2 was achieved for this jet velocity, again at an orifice-to-target spacing of 3 jet diameters, relative to the CHF of 21.9 W/cm^2 in the pool boiling configuration. These comparisons at both high (V_j = 9 m/s) and low (V_j = 1 m/s) jet velocities across a range of confinement heights confirm that nucleate boiling is the predominant mechanism that governs the two-phase jet impingement heat transfer and that the fully boiling regime heat transfer coefficient is insensitive to the presence or characteristics of the impinging jet, within the range of conditions considered here.

3.3 Discussion

The close match of confined jet impingement heat transfer in the fully boiling regime with pool boiling demonstrates that nucleate boiling is the dominant heat transfer mechanism in this regime. This conclusion is supported by the mapping of the flow field during confined, two-phase jet impingement performed by Rau *et al.* [25]. The radially outward wall jet flow, which governs the single-phase convection heat transfer behavior, was observed in that study to be completely disrupted by bubble nucleation due to boiling. Upon the onset of boiling, the flow field in the confinement gap becomes dominated by the vapor buoyancy as in pool boiling, rather than the inertia of the jet. In the case of the highest jet velocity (V_j = 9 m/s) and lowest orifice-to-target spacing (H/d = 0.5), the degradation of performance is likely due to vapor confinement, and is not a wall jet effect.

To observe the vapor formation characteristics in the confinement gap, Figure 5 compares high-speed video frames acquired during the current jet impingement experiments using an orifice-to-target spacing of 3 jet diameters and jet exit velocities of 1, 3, 6, and 9 m/s. Due to the dependence of flow boiling on the inlet mass flow rate and liquid subcooling, comparison across these cases is made on the basis of a non-dimensional heat input (Bl^*), defined in Ref. [25] as

$$Bl^* = \frac{qA}{\dot{m}C_p\left(T_{sat} - T_j\right)}$$

which is analogous to the Boiling number ($Bl = qA/\dot{m}h_{fg}$).

The heat flux cases chosen for comparison in Figure 5 correspond to a constant non-dimensional heat input of 0.76. At a constant non-dimensional heat input, the equilibrium thermodynamic quality of the fluid exiting the gap is fixed. Corresponding heat fluxes for each jet velocity are highlighted in the boiling curves shown in Figure 5. In the high-speed video frames in Figure 5, vapor bubbles appear to generally rise vertically from the surface of the heater, rather than being entrained into the radially outward liquid flow; only for the highest velocity case of 9 m/s are bubbles observed to slightly extend past the edges of the heater. Full videos, from which these frames were taken, are included in the Supplementary Materials. From this qualitative observation, we can infer that the wall jet appears to be disrupted by bubble nucleation at the heated surface, in agreement with the flow field mapping of Rau *et al.* [25]. Even though the highest jet velocity provides greater momentum, and therefore may better displace vapor being generated at the heater surface and hence extends CHF, the boiling curve corresponding to this case in Figure 2(a) still converges to an extension of the pool boiling data.

4 Conclusions

Direct experimental comparison of pool boiling and confined jet impingement heat transfer performance allows a delineation of the influence of the impinging jet on boiling behavior in the fully boiling regime. Over the range of jet velocities ($1 \leq V_j \leq 9\ m/s$) and orifice-to-target spacings ($0.5 \leq H/d \leq 10$) tested, the impinging jet is found to increase single-phase performance and extend the critical heat flux well beyond pool boiling limits. However, the fully boiling regime heat transfer coefficient is found to be insensitive to the presence of the jet. Jet impingement heat transfer performance is either identical to that of pool boiling or coincides with an extension of the correlated pool boiling heat transfer coefficient above the pool boiling critical heat flux, indicating that nucleate boiling is the dominant heat transfer mechanism in this regime; the convective effects of the jet play a negligible role. This result is likely due to the disruption of the wall jet formed during impingement by bubble nucleation at the heater surface.

Critical heat flux for confined jet impingement is found to increase linearly with increasing jet velocity, which differs significantly from the commonly reported cube-root dependence for free surface and submerged jet impingement configurations. Additionally, a decrease in both the boiling heat transfer coefficient and critical heat flux is observed for the highest jet velocity (V_j = 9 m/s) under highly confined conditions (H/d = 0.5). Otherwise, critical heat flux is insensitive to changes in the orifice-to-target spacing.

Acknowledgements

Financial support for this work provided by members of the Cooling Technologies Research Center, a graduated National Science Foundation Industry/University Cooperative Research Center at Purdue University, is gratefully acknowledged.

References

[1] M. J. Rau and S. V. Garimella, "Two-phase jet impingement: liquid-vapor interactions and heat transfer mapping for multiscale surface enhancement design," *Encyclopedia of Two-Phase Heat Transfer and Flow*, vol. 2. 2018.

[2] D. T. Vader, F. P. Incropera, and R. Viskanta, "Convective nucleate boiling on a heated surface cooled by an impinging, planar jet of water," *J. Heat Transf.*, vol. 114, no. 1, pp. 152–160, 1992.

[3] C. S. K. Cho and K. Wu, "Comparison of burnout characteristics in jet impingement cooling and stray cooling," in the Proceedings of the 1988 National Heat Transfer Conference, vol. 96, pp. 561–567, 1988.

[4] M. J. Rau and S. V. Garimella, "Local two-phase heat transfer from arrays of confined and submerged impinging jets," *Int. J. Heat Mass Transf.*, vol. 67, pp. 487–498, 2013.

[5] C. Mira-Hernández, M. D. Clark, J. A. Weibel, and S. V. Garimella, "Development and validation of a semi-empirical model for two-phase heat transfer from arrays of impinging jets," *Int. J. Heat Mass Transf.*, vol. 124, pp. 782–793, 2018.

[6] D. H. Wolf, F. P. Incropera, and R. Viskanta, "Local jet impingement boiling heat transfer," *Int. J. Heat Mass Transf.*, vol. 39, no. 7, pp. 1395–1406, 1996.

[7] Y. Katto and M. Kunihiro, "Study of the mechanism of burn-out in boiling system of high burn-out heat flux," *Bull. JSME*, vol. 16, no. 99, pp. 1357–1366, 1973.

[8] C. F. Ma and A. E. Bergles, "Boiling jet impingement cooling of simulated microelectronic chips," in Heat Transfer in Electronic Equipment 1983, vol. 28, pp. 5–12, 1983.

[9] C. F. Ma and A. E. Bergles, "Jet impingement nucleate boiling," *Int. J. Heat Mass Transf.*, vol. 29, no. 8, pp. 1095–1101, 1986.

[10] C. L. Struble and L. C. Witte, "An in situ technique for measuring heat transfer from a power transistor to a boiling liquid," *J. Heat Transf.*, vol. 116, no. 2, pp. 495–498, 1994.

[11] D. W. Zhou and C. F. Ma, "Local jet impingement boiling heat transfer with R113," *Heat Mass Transf.*, vol. 40, no. 6–7, pp. 539–549, 2004.

[12] 3M, 3M Novec Engineered Fluid HFE-7100 for Heat Transfer, 3M, St. Paul, MN, 2002, pp.1-8.

[13] M. J. Rau and S. V. Garimella, "Confined jet impingement with boiling on a variety of enhanced surfaces," *J. Heat Transf.*, vol. 136, no. 10, pp. 101503 1–12, 2014.

[14] G. K. Morris and S. V. Garimella, "Orifice and impingement flow fields in confined jet impingement," *J. Electron. Packag.*, vol. 120, no. 1, pp. 68–72, 1998.

[15] A. Bar-Cohen and T. W. Simon, "Wall superheat excursions in the boiling incipience of dielectric fluids," *Heat Transf. Eng.*, vol. 9, no. 3, pp. 19–31, 1988.

[16] P. J. Marto and V. J. Lepere, "Pool boiling heat transfer from enhanced surfaces to dielectric fluids," *J. Heat Transf.*, vol. 104, no. 2, pp. 292–299, 1982.

[17] S. M. You, A. Bar-Cohen, and T. W. Simon, "Boiling incipience and nucleate boiling heat transfer of highly wetting dielectric fluids from electronic materials," *IEEE Trans. Compon. Hybrids Manuf. Technol.*, vol. 13, no. 4, pp. 1032–1039, 1990.

[18] S. V. Garimella, "Heat transfer and flow fields in confined jet impingement," *Annu. Rev. Heat Transf.*, vol. 11, no. 11, pp. 413–494, 2000.

[19] M. G. Cooper, "Heat flow rates in saturated nucleate pool boiling-A wide-ranging examination using reduced properties," *Adv. Heat Transf.*, vol. 16, pp. 157–239, 1984.

[20] K. Stephan and M. Abdelsalam, "Heat-transfer correlations for natural convection boiling," *Int. J. Heat Mass Transf.*, vol. 23, no. 1, pp. 73–87, 1980.

[21] D. H. Wolf, F. P. Incropera, and R. Viskanta, "Jet impingement boiling," in P. H. James, F. I. Thomas (Eds.), Advances in Heat Transfer, Elsevier, vol. 23, pp. 1–132, 1993.

[22] L. Qiu, S. Dubey, F. H. Choo, and F. Duan, "Recent developments of jet impingement nucleate boiling," *Int. J. Heat Mass Transf.*, vol. 89, pp. 42–58, Oct. 2015.

[23] I. Mudawar and D. C. Wadsworth, "Critical heat flux from a simulated chip to a confined rectangular impinging jet of dielectric liquid," *Int. J. Heat Mass Transf.*, vol. 34, no. 6, pp. 1465–1479, 1991.

[24] S. V. Garimella and R. A. Rice, "Confined and submerged liquid jet impingement heat transfer," *J. Heat Transf.*, vol. 117, no. 4, pp. 871–877, 1995.
[25] M. J. Rau, T. Guo, P. P. Vlachos, and S. V. Garimella, "Stereo-PIV measurements of vapor-induced flow modifications in confined jet impingement boiling," *Int. J. Multiph. Flow*, vol. 84, pp. 19–33, 2016.

List of Tables

List of Figures

Table 1. Geometrical parameters and operating conditions for the two-phase jet impingement experiments.

d (mm)	$\dot{V}$ (ml/min)	V_j (m/s)	Re	H/d	ΔT_{sub} (°C)	p_{op} (kPa)
2	1,700	9	69,300	10, 3, 1, 0.5	8	101.3
	1,140	6	46,500	3		
	568	3	23,200	3		
	190	1	7,700	10, 3, 1, 0.5		

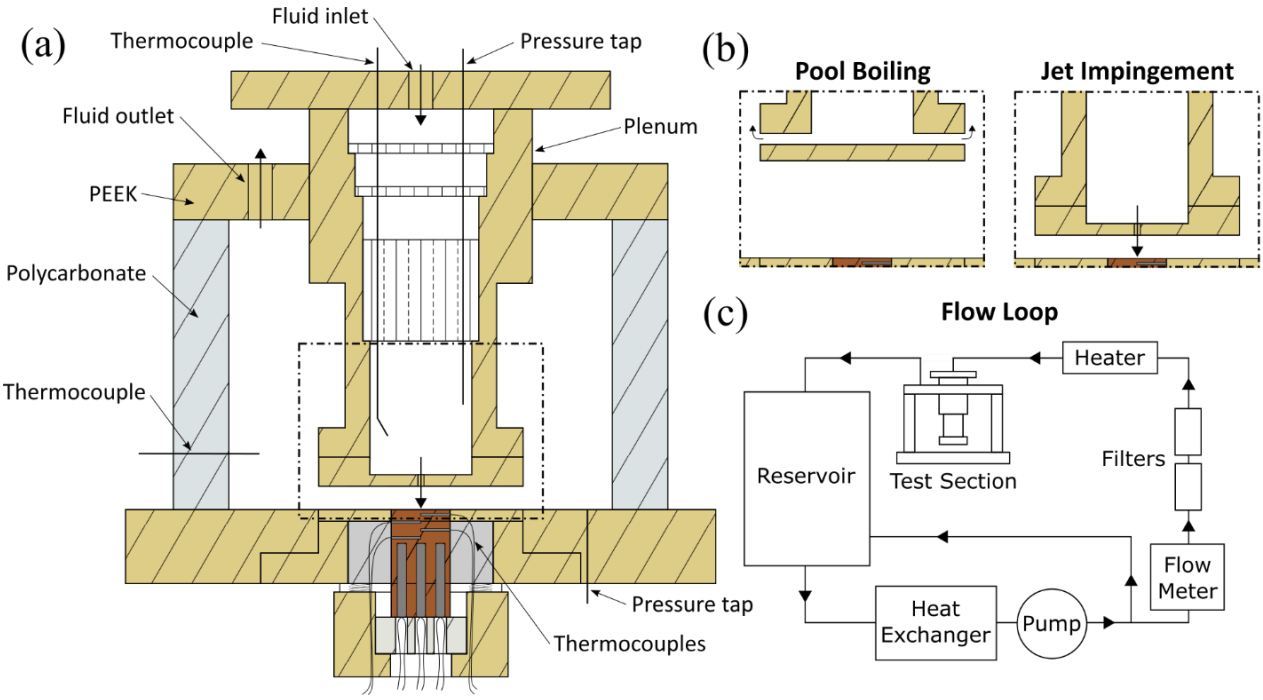

Figure 1. (a) Cross-sectional view of the test section, (b) schematic diagram of the orifice plate configuration for jet impingement and pool boiling, and (c) flow loop diagram.

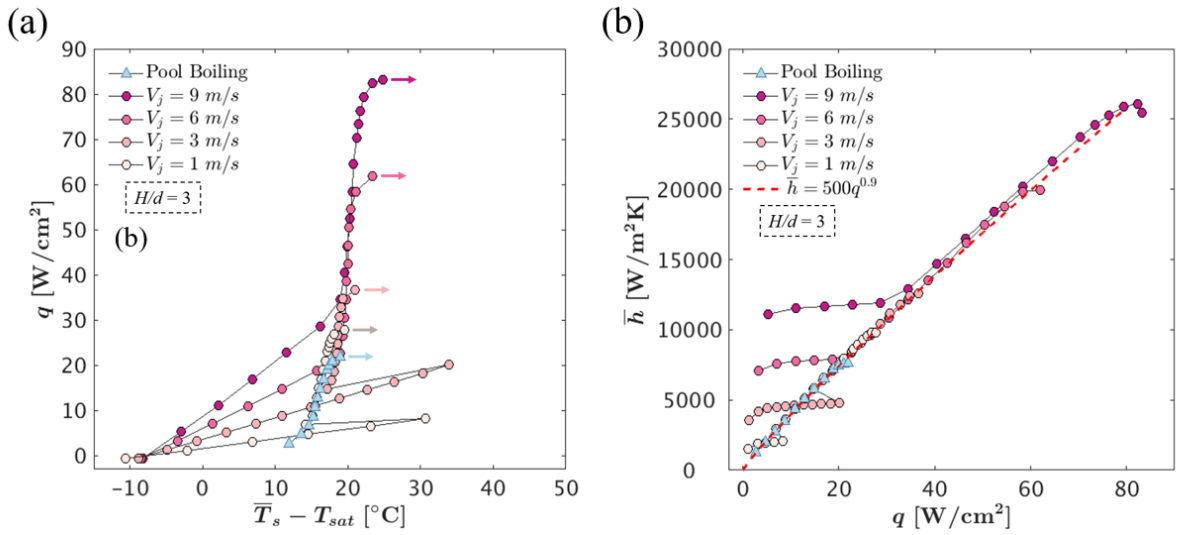

Figure 2. (a) Boiling curves and (b) heat transfer coefficients as a function of heat flux for the jet impingement configuration (corresponding to V_j = 1 m/s, 3 m/s, 6 m/s, and 9 m/s; H/d = 3) compared with pool boiling.

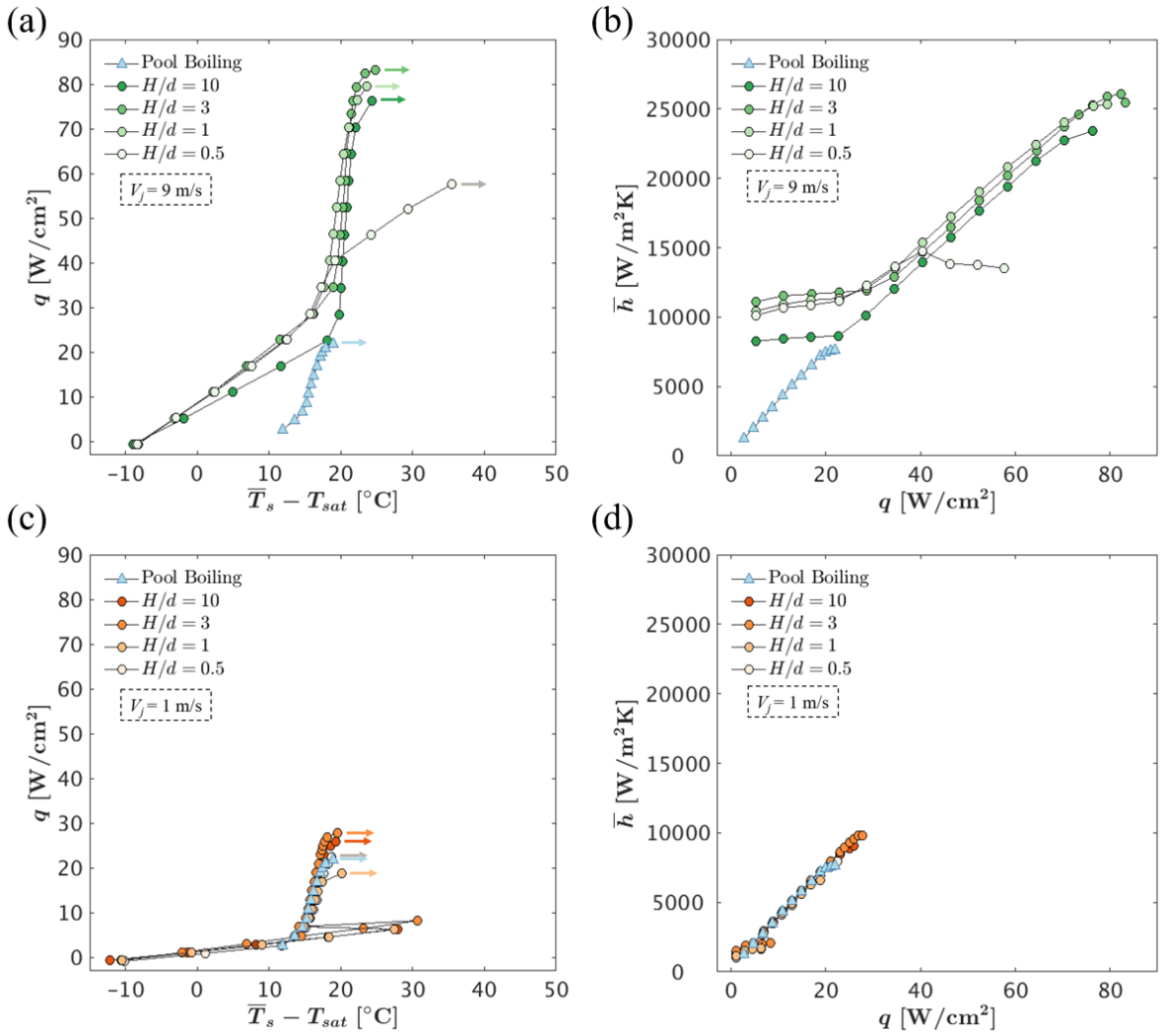

Figure 3. (a and c) Boiling curves and (b and d) heat transfer coefficients as a function of heat flux for the jet impingement configuration (corresponding to V_j = 9 m/s and 1 m/s, respectively; H/d = 0.5, 1, 3, and 10) compared with pool boiling.

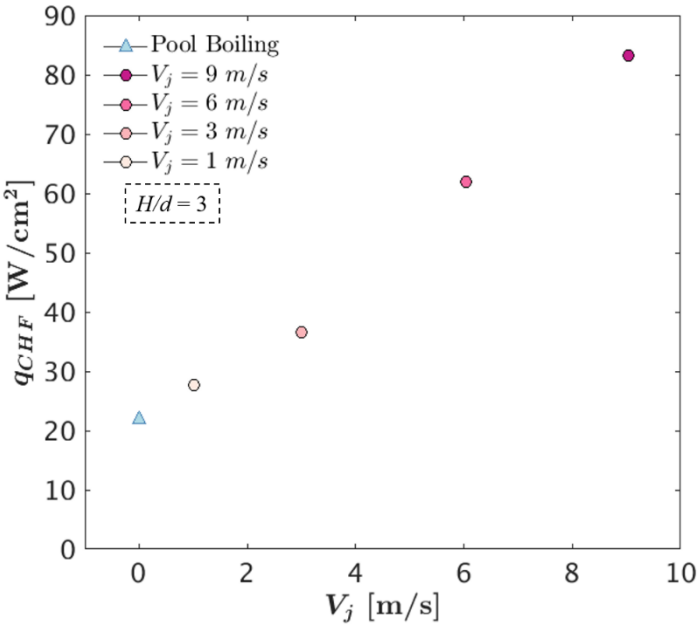

Figure 4. Critical heat flux (CHF) for the jet impingement (corresponding to V_j = 1 m/s, 3 m/s, 6 m/s, and 9 m/s; H/d = 3) and pool boiling configurations.

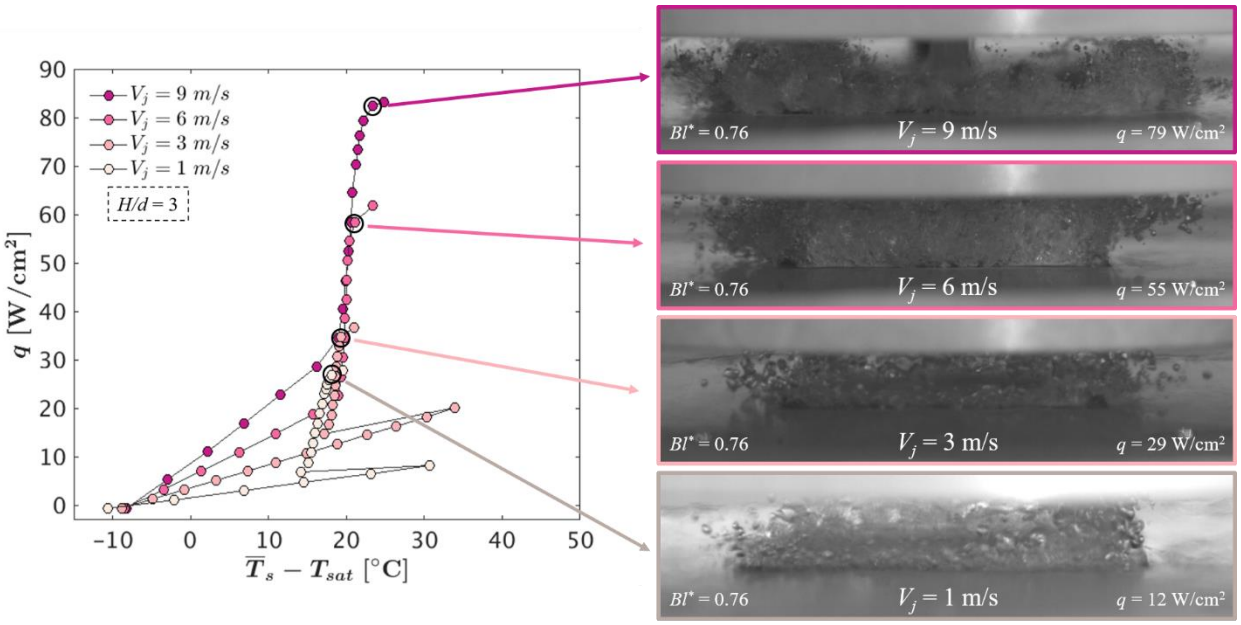

Figure 5. Comparison of high-speed video frames across four jet velocities (V_j = 1 m/s, 3 m/s, 6 m/s, and 9 m/s; H/d = 3) at a constant non-dimensional heat input (Bl^* = 0.76). The corresponding heat fluxes for each jet velocity are highlighted on the boiling curve. Full videos are included in the Supplementary Materials.